Archives of Biochemistry and Biophysics 583 (2015) 120–129

Contents lists available at ScienceDirect

Archives of Biochemistry and Biophysics

journal homepage: www.elsevier.com/ locate/yabbi

Exploring biochemical and functional features of *Leishmania major* phosphoenolpyruvate carboxykinase

Máximo Hernán Sosa, Lucila Giordana, Cristina Nowicki*

Instituto de Química y Fisicoquímica Biológica IQUIFIB-CONICET, Facultad de Farmacia y Bioquímica, Universidad de Buenos Aires, Junín 956, C1113AAD, Buenos Aires, Argentina

ARTICLE INFO

Article history:
Received 5 February 2015
Received in revised form
20 July 2015
Accepted 22 July 2015
Available online 11 August 2015

Keywords:
Leishmania parasites
Phosphoenolyruvate carboxykinase
3-Mercaptopicolinic acid
Mutagenesis studies

ABSTRACT

This work reports the first functional characterization of leishmanial PEPCK. The recombinant *Leishmania major* enzyme (Lmj_PEPCK) exhibits equivalent k_{cat} values for the phosphoenolpyruvate (PEP) and oxaloacetate (OAA) forming reactions. The apparent K_m towards OAA is 10-fold lower than that for PEP, while the K_m values for ADP and ATP are equivalent. Mutagenesis studies showed that D241, D242 and H205 of Lmj_PEPCK like the homologous residues of all known PEPCKs are implicated in metal ions binding. In contrast, the replacement of R43 for Q nearly abolishes Lmj_PEPCK activity. Moreover, the Y180F variant exhibits unchanged K_m values for PEP, Mn^{2+}, and HCO_3^-, being the k_{cat} for PEP- but not that for OAA-forming reaction more notably decreased. Instead, the Y180A mutant displays an increase in the K_m value towards Mn^{2+}. Therefore in Lmj_PEPCK, Y180 seems to exert different functions to those of the analogous residue in ATP- and GTP-dependant enzymes. Besides, the guanidinium group of R43 appears to play an essential but yet unknown role. These findings promote the need for further structural studies to disclose whether Y180 and R43 participate in the catalytic mechanism or/and in the transitions between the open and the catalytically competent (closed) forms of Lmj_PEPCK

1. Introduction

Leishmania parasites are pathogenic protozoa comprised within the family Trypanosomatidae, which also includes other human pathogens such as *Trypanosoma cruzi* and *Trypanosoma brucei*. Notably, more than 20 species of *Leishmania* are responsible for producing a broad spectrum of clinical manifestations in man (leishmaniasis), ranging from self-healing cutaneous lesions to debilitating mucocutaneous and lethal visceral infections. If untreated, leishmaniasis can lead to severe tissue damage, disfigurement and death. Up to now, no vaccines have been developed and the current clinical treatments are far from being satisfactory [1,2]. In mammals, *Leishmania* parasites are obligate intracellular pathogens, amastigotes proliferate within acidic vacuoles inside macrophages. Therefore, this developmental stage represents the target of anti-parasite therapies.

Phosphoenolpyruvate carboxykinases (PEPCKs) catalyzes oxaloacetate (OAA) decarboxylation and phosphoryl transfer from a nucleoside triphosphate (NTP) to form phosphoenolpyruvate (PEP). Even though this reaction is reversible *in vitro*, PEP formation is normally favored *in vivo*. In man two isoforms are active; one is localized in the cytosol and the other in the mitochondria. Given that the cytosolic PEPCK catalyzes the rate-controlling step in the gluconeogenic pathway, this isozyme has been the most deeply studied. In addition, cytosolic PEPCK also plays an important function in regulating energy homeostasis and flux through the TCA cycle [3].

Based on the specificity of PEPCKs towards the NTP utilized as energy donor, these enzymes are classified in two groups, ATP- and GTP-dependant proteins. Homologues from bacteria, yeast, plant and trypanosomatids use ATP, while PEPCKs from mammals and certain bacteria such as *Mycobacterium tuberculosis* counterpart utilize GTP. Both types of PEPCKs display remarkably low overall sequence relatedness (identity <20%). However, structural studies on PEPCKs from varied sources have shown that the key residues involved in the catalytic mechanism are reasonably conserved among ATP- and GTP-dependant enzymes [for review see [4–6]].

While a wide range of studies have been conducted to disclose the physicochemical properties, 3-D structures and metabolic roles of PEPCKs from diverse organisms, limited information is available for homologues from pathogenic trypanosomatids. Only *T. cruzi* and

* Corresponding author.
E-mail address: cnowicki@qb.ffyb.uba.ar (C. Nowicki).

http://dx.doi.org/10.1016/j.abb.2015.07.015
0003-9861/

T. brucei PEPCKs have been functionally characterized so far, and notably both enzymes differ in their kinetic parameters [7–9]. The 3-D structure of *T. cruzi* PEPCK has been solved in the absence of substrates or metal ions. Despite this fact, the conformation of the crystallized enzyme resembled that of the closed, ligand-bound form of *Escherichia coli* PEPCK [10].

In trypanosomatids, PEPCK localizes within glycosomes (peroxisome-like organelles), and like the mammalian homologues, it is also expected to be involved in gluconeogenesis and anaplerotic processes. However in these pathogenic protozoa, the reactions catalyzed by PEPCK take part in uniquely organized pathways [11]. This enzyme plays a major role in maintaining NAD^+/NADH and ATP/ADP balance *via* the glycosomal succinate fermentation pathway (gSF). PEPCK catalyzes the first committed step of the gSF by converting PEP into OAA. The subsequent transformation of OAA into succinate allows the reoxidation of two molecules of NADH into NAD^+, per molecule of PEP. Moreover, the generated C4 dicarboxylic acids (malate and succinate) are further utilized for Krebs cycle anaplerosis. On the other hand, PEPCK also participates in gluconeogenesis by means of the conversion of the OAA derived from amino acid catabolism into PEP. Both roles are supported by genetic and metabolic studies performed in the insect and mammalian stages of *Leishmania mexicana* [12–14]. Besides, recent findings have demonstrated that PEPCK is an essential enzyme for the survival of the mammalian stage of *T. brucei* [15].

Early studies have shown that the specific activity of PEPCK was about 6-fold higher in cell-free extracts of *L. mexicana* amastigotes than in the crude extracts of promastigotes, the insect stage of these parasites [16]. In line with those findings, proteomic approaches have also provided evidence for the presence of PEPCK in amastigotes from different *Leishmania* species [17–19]. However, no leishmanial PEPCK has been purified to protein homogeneity and none has been functionally characterized yet.

Taking advantage of the completely sequenced genomes of various *Leishmania* species, we cloned and functionally characterized *Leishmania major* PEPCK. Moreover, to further explore the functional properties of *L. major* PEPCK, the kinetic consequences of the replacement of seven strictly conserved residues in the ATP- and GTP-dependant homologues were also examined. Our results show that in regards to the kinetic properties, the recombinant *L. major* enzyme more closely resembles *T. brucei* than *T. cruzi* PEPCK. Interestingly, *L. major* PEPCK also differs from *T. cruzi* homologue in that 3-mercaptopicolinic acid (3MPA), a typical inhibitor of PEPCKs acts by means of a mixed and a non-competitive mechanism when PEP or HCO_3^- are tested as substrates, respectively. Moreover, mutagenesis studies suggest that as compared with the ATP- and GTP-dependant enzymes, Y180 and R43 might be differently involved either in the transitions between the open and closed forms or in the catalytic mechanism of *L. major* PEPCK.

2. Material and methods

2.1. PCR and cloning

Total DNA from *L. major* promastigotes was isolated [20]. *L. major PEPCK* (*LmjF.27.1810*, Lmj_*PEPCK*) was amplified by PCR using genomic DNA as template and *Pfu*-Turbo DNA-polymerase (Stratagene). In order to perform the PCR, specific primers were designed on the basis of the predicted ORF in the genome project database (http://www.genedb.org): *Lmj_pepck-fw-NdeI*: 5′-CATATGGCCCCGATCATCCAC-3′ and *Lmj_pepck-rev-EcoRI*: 5′-GAATTCCTACAGATGAGCCGTCTCC -3′. The PCR reaction settings were as follows: 5 min at 95 °C and 25 cycles under the next conditions: (i) denaturation at 95 °C for 45 s, (ii) annealing at 58 °C during 45 s, (iii) extension at 72 °C for 1 min 40 s, in addition a final extension step was performed for 10 min. The resulting DNA fragments were cloned into pGEM-T Easy vector and fully sequenced to confirm the predicted ORF. The DNA fragment encoding Lmj_*PEPCK* was excised by digestion with NdeI and EcoRI and ligated into pET28 vector. The generated pET28-Lmj_*PEPCK* plasmid allowed the expression of the recombinant PEPCK with a 6xHis extension at its N-terminus. Besides, in order to produce an untagged recombinant enzyme, Lmj_*PEPCK* was cloned into pET24 vector. Subsequently, the constructed plasmids were used to transform *E. coli* Rosetta (DE3) pLysS. A selected bacteria colony was grown at 37 °C in LB medium supplemented with 30 μg/ml kanamycin and 34 μg/ml chloramphenicol. When an OD_{600nm} of 0.6 was reached, protein expression was induced by adding isopropyl-D-thiogalactopyranoside at final concentration of 0.1 mM. Then, cultures were further grown overnight at 20 °C. The recombinant His-tagged Lmj_PEPCK was purified by affinity chromatography on a Ni^{2+}-nitrilotriacetic (Ni-NTA) column (Qiagen, Germany) following standard procedures. Instead, the untagged enzyme was purified by cation exchange and gel filtration chromatography. The bacteria cell-free extract was applied onto a cation exchange matrix equilibrated in 75 mM triethanolamine buffer, pH 7.4. The weakly interacting proteins were washed with the same buffer while bound proteins were eluted with a linear gradient from 0 to 500 mM KCl in the same buffer. Lmj_PEPCK eluted at about 300 mM of KCl. Subsequently, the fractions with the highest specific activities were pooled and subjected to gel filtration chromatography on a Sephacryl-S200 HR column equilibrated with 50 mM HCl-Tris buffer, pH 8, supplemented with 150 mM NaCl. Protein homogeneity of the recombinant Lmj_PEPCK was analyzed by SDS-PAGE [21], and protein concentration was determined using the method of Bradford and bovine serum albumin as standard [22]. The N-terminal sequence of the recombinant untagged protein was determined by Edman degradation in an Automatic Sequencer (Applied Biosystems, Foster City, CA, USA), run according to the manufacturer's instructions at Lanais-Pro (UBA-CONICET).

2.2. PEPCK activity assays

PEPCK activity was measured spectrophotometrically by monitoring the absorbance decrease at 340 nm resulting from NADH oxidation in the carboxylation and decarboxylation assays. The reactions in both directions were conducted in 75 mM triethanolamine (TEA) buffer, pH 7.4 at 37 °C. PEP-carboxylation was followed by coupling the production of oxaloacetate to NADH oxidation in the presence of malate dehydrogenase. A typical assay mixture contained 2 mM ADP, 6 mM PEP, 100 mM $NaHCO_3^-$, 3.5 mM $MgCl_2$, and 0.15 mM $MnCl_2$, 0.28 mM NADH, 8 units of malate dehydrogenase. The PEP-carboxylation reaction was started by adding Lmj_PEPCK. On the other hand, the standard assay mixture of the OAA-decarboxylation reaction contained 1 mM ATP, 1 mM OAA, 3.5 mM $MgCl_2$, 0.15 mM $MnCl_2$, 0.28 mM NADH, and 20 units of both lactate dehydrogenase and pyruvate kinase. The OAA-decarboxylation reaction was started by adding OAA. For each reaction, blanks were run to measure the unspecific OAA decarboxylation. The obtained values were substracted from those measured in the presence of Lmj_PEPCK. One unit of enzyme activity was defined as the amount of enzyme that produces either 1 μmol of OAA or PEP per min. The optimal pH of the recombinant Lmj_PEPCK reaction was determined using a wide range of buffers: 75 mM sodium acetate/acetic acid (pH 3.6–5.6), 75 mM Bis-Tris (pH 5.8–7.2), 75 mM TEA-HCl (pH 7.3–8.3), and 75 mM glycine-sodium hydroxide, (pH 8.6–10.6). Initial velocity studies were performed by varying the concentration of one of the substrates around its K_m value while the concentrations of the other substrates were maintained constant at saturating levels. The kinetic parameters

were determined from at least three to four data sets which were adjusted to non-linear regression by using GraphPad Prism 5.01 software. Turnover numbers (k_{cat}, s^{-1}) were calculated using a molecular mass of 58.2 kDa per subunit. To examine the inhibition modality of (3MPA), steady state kinetic data were obtained at different concentrations of the inhibitor. The plots of velocity versus [S] at several fixed 3MPA concentrations were globally fitted to different models (competitive, non-competitive, mixed and uncompetitive) using GraphPad 5.01 software and the equations stated below:

Competitive

$$v = \frac{V_{max}[S]}{[S] + K_m\left(1 + \frac{[I]}{K_i}\right)}$$

Noncompetitive

$$v = \frac{\frac{V_{max}}{\left(1 + \frac{[I]}{K_i}\right)}[S]}{[S] + K_m}$$

Mixed

$$v = \frac{\frac{V_{max}}{\left(1 + \frac{[I]}{\alpha K_i}\right)}[S]}{[S] + K_m\frac{\left(1 + \frac{[I]}{K_i}\right)}{\left(1 + \frac{[I]}{\alpha K_i}\right)}}$$

Uncompetitive

$$v = \frac{\frac{V_{max}}{\left(1 + \frac{[I]}{\alpha K_i}\right)}[S]}{[S] + K_m\left(1 + \frac{[I]}{\alpha K_i}\right)}$$

The inhibition type was determined on the bases of the statistical goodness of fits (Akaike information criterion, AICc values) of the experimental data to the alternative kinetic models. The equation used for this purpose is included below:

$$AIC_C = N\ln\left(\frac{SS}{N}\right) + 2K + \frac{2K\,(K+1)}{N-K-1}$$

where "N" is the number of data points, "K" is the number of parameters fit by the regression plus one and *SS* is the sum of the square of vertical distances of points from the curve [23,24]. On the other hand, the inhibition type was also estimated by Lineweaver-Burk plots and the K_{is} and K_{ii} values were calculated from the graphs of slopes and intercepts, respectively, as a function of the tested concentrations of 3MPA.

2.3. Site directed mutagenesis

Complementary oligonucleotides containing the appropriate base alterations (in bold) were designed according to Lmj_*PEPCK* sequence (Supplementary material, Table 1). Mutants were constructed following Quick Change protocol. PCRs were carried out with *Pfu*-Turbo DNA polymerase high fidelity and pET28-Lmj_*PEPCK* was used as template. The PCR products were digested with DpnI and the resulting DNA was used to transform XL1-Blue *E. coli* competent cells. Each mutation was confirmed by DNA sequencing.

2.4. Circular dichroism spectroscopy

CD spectra were recorded with a Jasco 810 spectropolarimeter. Analyses in the Far-UV region were conducted at the wavelength range between 200 and 250 nm, in 0.1-cm quartz cuvettes at 25 °C. The wild type Lmj_PEPCK and the constructed variants were desalted in 50 mM buffer HCl-Tris, pH 7.9, containing 50 mM NaCl, the final protein concentration was in the range of 0.3 mg ml^{-1}. For near-UV CD spectra, the wavelength range was 250–350 nm, the analyzed proteins were dissolved in the aforementioned buffer, at final concentration of 0.9 mg ml^{-1}, and the path length was 1.0 cm. In all cases data were acquired at a scan speed of 20 nm min^{-1} and at least 3 scans were averaged for each sample. Blank scans were substracted from the spectra and values of ellipticity were expressed in units of deg cm^2 $dmol^{-1}$. Data analysis was carried out using GraphPad Prism 5.01 software.

2.5. Fluorescence spectroscopy

Fluorescence measurements were performed on a Jasco FP-6500 spectrofluorometer operating in the ratio mode and equipped with a thermostated cell holder connected to a circulating water bath set at 20 °C. The intrinsic fluorescence (IF) of the recombinant wild-type Lmj_PEPCK and that of the constructed mutants was measured in 50 mM HCl-Tris buffer, pH 7.9, supplemented with 50 mM NaCl. Protein concentration was in the range of 0.2 mg ml^{-1}. Excitation wavelength was set at 295 nm and emission data were collected in the range 310–410 nm. A 1.0 cm path length cell sealed with a Teflon cap was used and the spectral slit-width was set to 3 nm for both monochromators.

2.6. Molecular modeling of L. major PEPCK

The homology model of *L. major* PEPCK was constructed by comparative modeling of the crystallographic data of *E. coli* and *T. cruzi* PEPCKs (PDB: 2PXZ and 1II2, respectively) using MODELLER 9.12 software. The obtained model of *L. major* PEPCK was validated by using Procheck [25] and Verify 3D [26] programs. Structure alignment was conducted with UCSF Chimera 1.5.3 (https://www.cgl.ucsf.edu/chimera/) [27] and ESPrit 3.0 web tool (http://espript.ibcp.fr/ESPript/ESPript/) [28].

3. Results

3.1. Heterologous expression

The survey of the sequenced genomes of *Leishmania* species revealed that *L. major* and *L. mexicana* exhibited two gene copies encoding putative PEPCKs, although other species such as *Leishmania infantum* and *Leishmania braziliensis* presented only a single copy for this gene. These putative leishmanial PEPCKs displayed nearly identical sequences, and high similarity with homologues from the closely related trypanosomes (identity ≅ 80%). Besides, these enzymes also presented lower but important relatedness with other ATP-dependant enzymes such as PEPCKs from *Saccharomyces cerevisiae* and *E. coli* (identity ≅ 51% and 42%, respectively). Given that PEPCK has not yet been purified from any *Leishmania* species, in order to explore the biochemical properties of this enzyme, we obtained the recombinant *L. major* PEPCK. The 6xHis tagged protein was purified by means of a single step of affinity

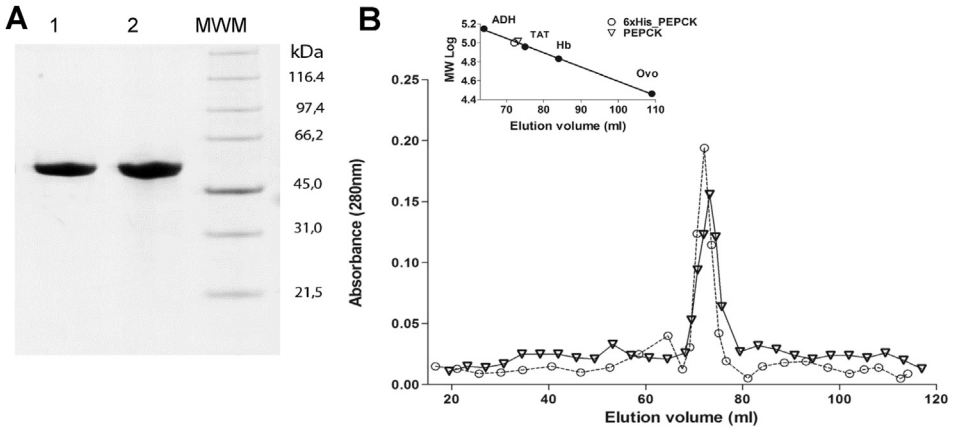

Fig. 1. Heterologous expression and purification of the putative phosphoenolpyruvate carboxykinase from *L. major*. **(A)** The recombinant 6xHis-tagged and untagged PEPCKs were expressed and purified as described in Material and Methods section. Each of the recombinant proteins (5 μg) were subjected to SDS-PAGE in 10% acrylamide gels under reducing conditions and were visualized by Coomassie Blue staining. Lane 1, 6xHis tagged-Lmj_PEPCK; Lane 2, untagged-Lmj_PEPCK; MWM, molecular mass standards. The mass values of the protein markers are given in kDa and shown on the right side of the panel. **(B)** The gel filtration chromatography in native conditions of *L. major* 6xHis tagged and untagged PEPCKs was performed through S-200 HR as described in Material and Methods section. The elution pattern of the 6xHis tagged enzyme is shown in open circles and that of the untagged protein in open triangles. The inset shows the standard curve for molecular mass, proteins used as molecular mass markers are indicated in dark circles: alcohol dehydrogenase (ADH, 146.8 kDa); tyrosine aminotransferase from *Trypanosoma cruzi* (TAT, 90 kDa); Hemoglobin (Hb, 68 kDa) and ovoalbumin (Ovo 44 kDA).

chromatography onto a Ni^{2+} charged NTA matrix, as described in Material and Methods section. The recombinant 6xHis tagged Lmj_PEPCK yielded 3 mg per liter of bacterial culture, and when stored at 4 °C, the enzyme was stable for several days with no evident loss of activity. Once the 6xHis tagged Lmj_PEPCK was analyzed by SDS-PAGE under denaturing conditions, a single band with the expected apparent molecular mass was visualized (≅59 kDa), (Fig. 1A). Also, in gel filtration chromatography, under native conditions the recombinant enzyme eluted in a single symmetric peak. The elution volume corresponded to a protein of approximately 103 kDa (Fig. 1B). This value fits in well with a dimeric organization of *L. major* enzyme.

Notably, as compared with the *T. cruzi* counterpart, the 6xHis tagged Lmj_PEPCK exhibited a significantly higher specific activity in the OAA-forming direction (69.6 ± 8 U mg^{-1} vs 3.2 ± 0.04 U mg^{-1}, anaplerotic reaction). The recombinant enzyme was also more active in the PEP-forming direction (gluconeogenic reaction), although in this case, the specific activity was only ≅2 -fold higher (51.6 ± 2 U mg^{-1} vs 28.04 ± 5.5 U mg^{-1}) [7]. The potential influence of the 6xHis tag on the catalytic competence of Lmj_PEPCK was examined by expressing the untagged enzyme in *E. coli*. Based on the fact that different pI values were predicted for *L. major* and *E. coli* PEPCKs (8.2 and 5.5, respectively) in addition to the dissimilar molecular organization of both homologues (dimer vs monomer), the untagged Lmj_PEPCK was separated from the endogenous bacteria enzyme by a two-step purification procedure. Briefly, the bacteria cell-free extract was applied onto a cation exchange matrix equilibrated with 75 mM triethanolamine buffer, pH 7.4, as described in Material and Methods section. Those fractions which eluted at about 300 mM of KCl and exhibited PEPCK activity were collected. The recombinant enzyme was further purified by gel filtration chromatography. The untagged Lmj_PEPCK obtained upon the latter step presented a molecular mass of about 100 kDa as well as being homogeneous when analyzed by SDS-PAGE (Fig. 1A). Moreover, the expected N-terminal sequence of Lmj_PEPCK was confirmed by Edman degradation of the first six amino acids from the recombinant protein. When tested in the carboxylation and decarboxylation reactions, the untagged enzyme displayed identical specific activity to that determined for the 6xHis tagged protein (not shown). Hereinafter, the 6xHis tagged Lmj_PEPCK was utilized for further kinetic characterization and mutagenesis studies.

3.2. Kinetic characterization

L. major PEPCK was active in a wide range of pH values (4.5–9.0); the enzyme was capable of catalyzing PEP carboxylation at lower pHs than OAA decarboxylation (not shown). However, for both reactions, the recombinant enzyme presented optimal activities at equivalent pH values (7.0–8.0). Therefore, 75 mM triethanolamine buffer, pH 7.4, was selected for activity measurements.

Similarly to PEPCKs from different sources, the *L. major* enzyme exhibited an absolute requirement for divalent cations. The most effective activator was Mn^{2+} (in low μM range) while Mg^{2+} enhanced catalysis synergistically, displaying an optimal activity at mM concentrations. Also, the Lmj_PEPCK proved to be active at low mM concentrations of other divalent cations. The level of preferences was estimated as follows: $Mn^{2+} \cong Co^{2+} >> Zn^{2+} > Ni^{2+} > Mg^{2+}$. Among the tested metal ions, Ca^{2+} and Cu^{2+} showed to be completely ineffective. On the other hand, the activity of Lmj_PEPCK remained unaltered when measured in the presence or absence of cysteine protective reagents such as 1 mM dithiothreitol (not shown).

Kinetic studies showed that the recombinant *L. major* PEPCK exhibited typical hyperbolic curves for all the assayed substrates (Supplementary material, Fig. 1). The apparent K_m values towards ADP and ATP were equivalent, while this apparent kinetic parameter for OAA was 10-fold lower than that determined for PEP. Besides, the apparent K_m value towards Mn^{2+} was in the μM range and the apparent k_{cat} values for the OAA- and PEP-forming reactions were similar (Table 1, panel A). As resulted from the lower apparent K_m for OAA than for PEP, the catalytic efficiency (k_{cat}/K_m) of the recombinant Lmj_PEPCK was about 9-fold higher in the PEP- than OAA-forming direction (gluconeogenic vs anaplerotic reactions).

Similarly to PEPCKs from diverse sources, 3MPA also exerted an inhibitory effect on *L. major* enzyme, equally decreasing the capability of catalyzing PEP and OAA production in a dose-dependent manner. The specific activities of Lmj_PEPCK were lowered to approximately 50% at 40 μM of 3MPA. To further evaluate the

Table 1
Kinetic characterization of the recombinant phosphoenolpyruvate carboxykinase from *L. major* and H205Q, Y180F and Y180A variants.

		Apparent kinetic parameters in the OAA-forming direction				Apparent kinetic parameters in the PEP-forming direction			
		Substrate	K_m (mM)	k_{cat} (s^{-1})	k_{cat}/K_m (M^{-1} s^{-1})	Substrate	K_m (mM)	k_{cat} (s^{-1})	k_{cat}/K_m (M^{-1} s^{-1})
Panel A	Wild type	PEP	0.90 ± 0.13	65.52 ± 3.14	(7.20 ± 0.14) × 10^4	OAA	0.09 ± 0.01	51.54 ± 2.2	(5.73 ± 0.11) × 10^5
		ADP	0.09 ± 0.01	78.82 ± 3.54	(8.76 ± 0.16) × 10^5	ATP	0.054 ± 0.006	48.09 ± 1.9	(8.91 ± 0.13) × 10^5
		Mn^{2+}	0.0068 ± 0.0007	60.01 ± 3.76	(8.57 ± 0.18) × 10^6	Mn^{2+}	0.008 ± 0.0002	50.73 ± 3.4	(6.34 ± 0.58) × 10^6
		HCO_3^-	12.30 ± 1.75	68.31 ± 4.39	(5.55 ± 0.11) × 10^3				
Panel B	PEPCK_H205Q	[a]PEP	1.63 ± 0.36	0.7 ± 0.04	(4.29 ± 1,19) × 10^2	[a]OAA	0.21 ± 0.03	4.41 ± 0.11	(2.10 ± 0.16) × 10^4
		[a]ADP	0.41 ± 0.06	0.67 ± 0.04	(1.63 ± 0.45) × 10^3	[a]ATP	0.15 ± 0.04	3.86 ± 0.15	(2.63 ± 0.85) × 10^4
		Mn^{2+}	1.93 ± 0.31	0.89 ± 0.03	(4.61 ± 0.89) × 10^2	Mn^{2+}	3.20 ± 0.75	3.43 ± 0.26	(1.07 ± 0.33) × 10^3
		[a]HCO_3^-	7.59 ± 0.91	0.64 ± 0.02	84.3 ± 12.7				
Panel C	PEPCK_Y180F	PEP	0.59 ± 0.05	37.78 ± 0.70	(6.36 ± 0.69) × 10^4	OAA	0.17 ± 0.03	9.07 ± 0.68	(5.46 ± 0.14) × 10^4
		ADP	0.10 ± 0.01	29.80 ± 0.56	(3.04 ± 0.32) × 10^5	ATP	0.09 ± 0.01	6.75 ± 0.16	(7.26 ± 0.83) × 10^4
		Mn^{2+}	0.009 ± 0.0018	30.87 ± 2.21	(3.43 ± 0.93) × 10^6	Mn^{2+}	0.0025 ± 0.0003	6.46 ± 0.31	(2.57 ± 0.40) × 10^6
		HCO_3^-	16.67 ± 2.20	31.52 ± 2.38	(1.89 ± 0.39) × 10^3				
Panel D	PEPCK_Y180A	[b]PEP	1.24 ± 0.14	2.66 ± 0.07	(2.15 ± 0.30) × 10^3	[b]OAA	0.43 ± 0.11	3.18 ± 0.27	(7.40 ± 2.52) × 10^3
		[b]ADP	0.29 ± 0.04	3.22 ± 0.13	(1.11 ± 0.20) × 10^4	[b]ATP	0.09 ± 0.02	3.93 ± 0.20	(4.23 ± 0.99) × 10^4
		Mn^{2+}	0.10 ± 0.02	3.34 ± 0.12	(3.34 ± 0.78) × 10^4	Mn^{2+}	0.14 ± 0.020	4.41 ± 0.25	(3.15 ± 0.63) × 10^4
		[b]HCO_3^-	13.97 ± 1.38	3.61 ± 0.11	(2.58 ± 0.33) × 10^2				

The kinetic parameters were determined by varying the concentration of the tested substrate whereas the concentrations of the other substrates were kept constant at the concentrations corresponding to the standard reaction mixture described in Material and Methods. The apparent K_m and V_{max} values were determined by non-linear regression using GraphPad Prism 5.01 software. The kinetic constants are the means of at least three to four determinations ± S.E.M. Turnover numbers (k_{cat}, s^{-1}) were calculated using a molecular mass of 58.2 kDa per subunit. [a] and [b] denotes those kinetic parameters which were determined at 10 mM and 1.5 mM of Mn^{2+}, respectively.

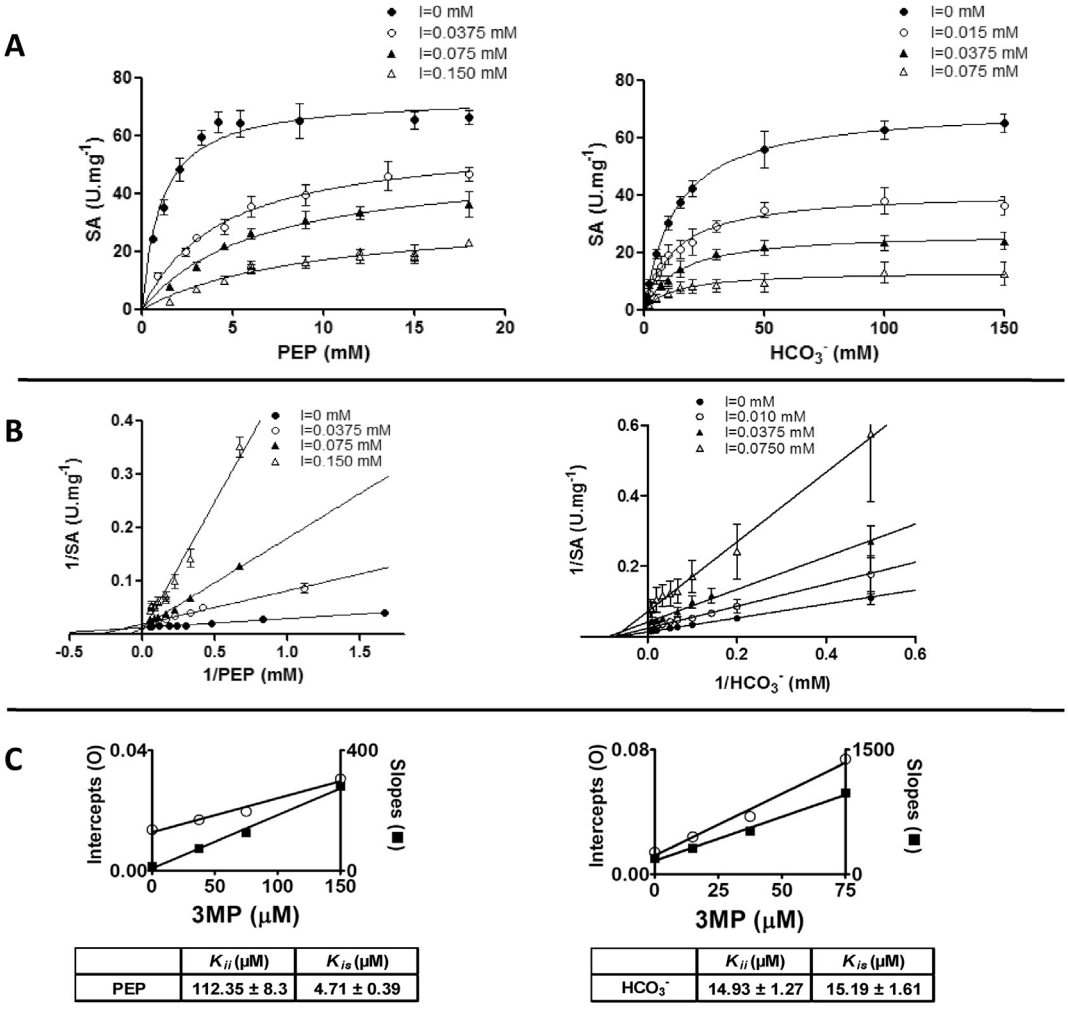

Fig. 2. The inhibitory effect of 3-mercaptopicolinic acid (3MPA) on the activity of *L. major* PEPCK. **(A)** The influence of 3MPA on the apparent K_m and V_{max} values when PEP and HCO_3^- were tested as substrates is illustrated with Michaelis-Menten plots. In regards to PEP (panel A, left) and HCO_3^- (panel A, right), the best fits were obtained for a mixed and a non-competitive model, respectively, when the Akaike information criterion (AIC_c) was applied (shown in Supplementary material, Table 2). **(B)** The corresponding Lineweaver-Burk plots for PEP and HCO_3^- are depicted in the left and right side panels, respectively. **(C)** Secondary replots of slopes and intercepts for PEP and HCO_3^- as a function of the assayed 3MPA concentrations are represented in the left and right panels, respectively. The estimated K_{ii} and K_{is} values for PEP and HCO_3^- are tabulated below each graph. The errors associated with each data point in the Michaelis–Menten and Lineweaver-Burk plots are indicated and the assayed concentrations of 3MPA are shown in the insets.

mechanism by which 3MPA inhibited Lmj_PEPCK, steady state kinetic studies were conducted and the initial rates of PEP-carboxylation reaction were measured at different concentrations of the inhibitor. The obtained data were analyzed by (i) fitting the untransformed data to the different kinetic models as described in Material and Methods section, (ii) constructing the double reciprocal graphs and further replots of the slopes and intercepts as a function of the assayed 3MPA concentrations. The outcomes obtained by applying the nonlinear regression supported a mixed inhibitory mechanism of 3MPA for PEP and a canonical non-competitive mechanism in respect to HCO_3^- (Fig. 2A). The lowest Akaike information criterion (AIC_c) values were used to select the best models (Supplementary material, Table 2). On the other hand, the Lineweaver-Burk plots also showed analogous inhibitory mechanisms for both substrates (Fig. 2B). Consistently, the secondary replots provided equivalent apparent K_{ii} and K_{is} values (14.93 μM and 15.19 μM, respectively) for HCO_3^-. However, in the case of PEP, these parameters were notably dissimilar, being K_{ii} higher than K_{is}. (112.35 μM vs 4.71 μM) (Fig. 2C). In brief, both methods (global fitting of untransformed data and double reciprocal graphical plots) estimated equivalent inhibition modalities of 3MPA towards *L. major* PEPCK, a mixed inhibition mechanism for PEP and a canonical non-competitive mechanism in respect to HCO_3^-.

On the other hand, regarding the non-physiological reactions catalyzed by certain PEPCKs such as OAA decarboxylation in the absence of ATP (OAA decarboxylase activity) or phosphoryl transfer from PEP to ADP (Pyruvate Kinase-like activity, PK-like), *L. major* PEPCK only displayed PK-like activity. For this secondary reaction, a specific activity of about 1.5 ± 0.3 U mg^{-1} was determined.

3.3. Mapping the active site of L. major PEPCK

A three-dimensional model of Lmj_PEPCK was built by using the 3-D structures of PEPCKs from *T. cruzi* and *E. coli* enzymes (1Il2.pdb and 2PXZ.pdb, respectively) as templates; a structure-based protein alignment is depicted in Fig. 3. In order to provide experimental evidence about the roles played by selected conserved residues in *L. major* PEPCK, seven single point mutants were obtained and functionally characterized. The first group of mutants was constructed to address whether the side chains of D241, D242 and H205 were indeed implicated in binding the Mn^{2+} and Mg^{2+} metal ions. Hence, the following variants were built: D241A, D242A and H205Q. Besides, the second group of mutations (R43Q, R43A, Y180A and Y180F; R65 and Y207 *E. coli* numbering) was designed to probe the potential functions of R43 and Y180 in the active site of *L. major* PEPCK. The Lmj_PEPCK variants were expressed in parallel with the wild type enzyme. Upon purification by affinity chromatography, the mutated proteins exhibited equivalent yields as well as presenting the expected apparent molecular masses, when analyzed in SDS-PAGE (not shown). However, the Lmj_PEPCK R43A variant was not functionally characterized given that this mutant resulted in a poorly stable protein with a manifest trend towards aggregation. The secondary and tertiary structure contents of Lmj_PEPCK Y180F, Y180A, D242A, D241A, R43Q and H205Q mutants were examined by spectroscopic analysis. As compared with the wild type enzyme, all the variants presented indistinguishable IF spectra and no significant changes in the near-UV CD patterns were observed (Fig. 4A and B). Furthermore, CD analysis in the far-UV region showed that the mutated proteins also exhibited equivalent patterns, when compared with the wild type enzyme (Fig. 4C). These outcomes indicated that the engineered substitutions neither altered the overall folding nor produced any significant distortion in the secondary and tertiary structures of the mutated proteins.

3.3.1. D241, D242 and H205 variants

All PEPCKs possess two strictly conserved aspartate residues in the Kinase-2 motif (^{265}LIGDD^{269}, *E. coli* sequence), which establish hydrogen bonds with water molecules as well as with other side chains from the active site and form part of the Mn^{2+} and Mg^{2+} binding sites. Among other side chains involved in the hydrogen bonding network, the imidazole group of H232 (*E. coli* numbering) also contributes to Mn^{2+} binding in the active site [4]. In *L. major*, the substitution of D242 for A led to a completely inactive enzyme (Fig. 4, panel D). Besides, identical substitution of D241 also exerted a large influence on the OAA- and PEP-forming activities (about 1400-fold and 31-fold, respectively). The operability of Lmj_PEPCK D241A and D242A mutants could not be rescued even though the concentrations of Mn^{2+} (enzyme cofactor) and Mg^{2+}were raised 100-fold in the standard reaction mixture. On the other hand, the substitution of H205 for Q (H232 in *E. coli*) also remarkably diminished the activity of this variant (Fig. 4, panel D). However, the capability of H205Q mutant to catalyze PEP- and OAA-forming reactions could be rescued when the concentration of Mn^{2+} was raised in the reaction mixture. Further kinetic analysis showed that when this mutant was assayed either in PEP- or OAA-forming reactions, only the apparent K_m value towards Mn^{2+} was dramatically increased (over 250-fold). Moreover, as compared with the wild type enzyme, the catalytic efficiency of H205Q variant was notably lower for the reaction leading to OAA production. This outcome resulted from a remarkable high decrease (100-fold) in the apparent k_{cat} values for OAA-forming activity (Table 1, panel B).

3.3.2. R43Q, Y180A and Y180F variants

The *L. major* PEPCK R43Q variant exhibited an extremely low activity either in the OAA- or PEP-forming directions. The decrease appeared to be notably higher for OAA-than for PEP-forming activities (≅31000-fold vs ≅1800-fold), (Fig. 4, panel D). The fact that the substitution of R43 for Q so remarkably influenced PEP and OAA forming capabilities indicated that like in other PEPCKs, the guanidinium group of R43 played a critical role in the catalytic mechanism. However, further characterization of this mutant was precluded because its activity remained almost unchanged even when the concentration of PEP, HCO_3^- and OAA was increased within the limits of substrate solubility. On the other hand, the role of Y180 in the catalytic mechanism of Lmj_PEPCK was explored by constructing two variants, Y180F and Y180A. The more conservative substitution (Y for F) exerted a milder effect on Lmj_PEPCK operability; as compared with the wild type enzyme, the specific activity of this mutant showed a 2- and 8-fold decrease for the OAA- and PEP-forming reactions, respectively (Fig. 4, panel D). Lmj_PEPCK Y180F mutant presented nearly unaltered apparent K_m values towards PEP, ADP, HCO_3^-, OAA and ATP. Besides, the apparent K_m value for Mn^{2+} also remained unchanged in the PEP- and OAA-forming directions. When compared with the wild type enzyme, the lower catalytic efficiency ($k_{cat}/K_m \approx$ 10-fold) observed in the decarboxylation of OAA mainly derived from the decrease in the k_{cat} value in PEP-forming reaction (Table 1, panel C). Besides, PK-like activity of Lmj-PEPCK Y180F variant remained unchanged (not shown) in comparison with the wild type enzyme. Instead, the replacement of Y180 for A brought about more important effects on the carboxylation and decarboxylation activities of Lmj_PEPCK (Fig. 4, panel D). The kinetic analysis of Y180A mutant indicated that the lack of this aromatic ring was mainly reflected in the apparent K_m value towards Mn^{2+}, which was about 10-fold higher than that determined for the wild type enzyme in the PEP- and OAA-forming directions. Besides, this variant exhibited equivalently reduced the k_{cat} values for the carboxylation and decarboxylation reactions (Table 1, panel D).

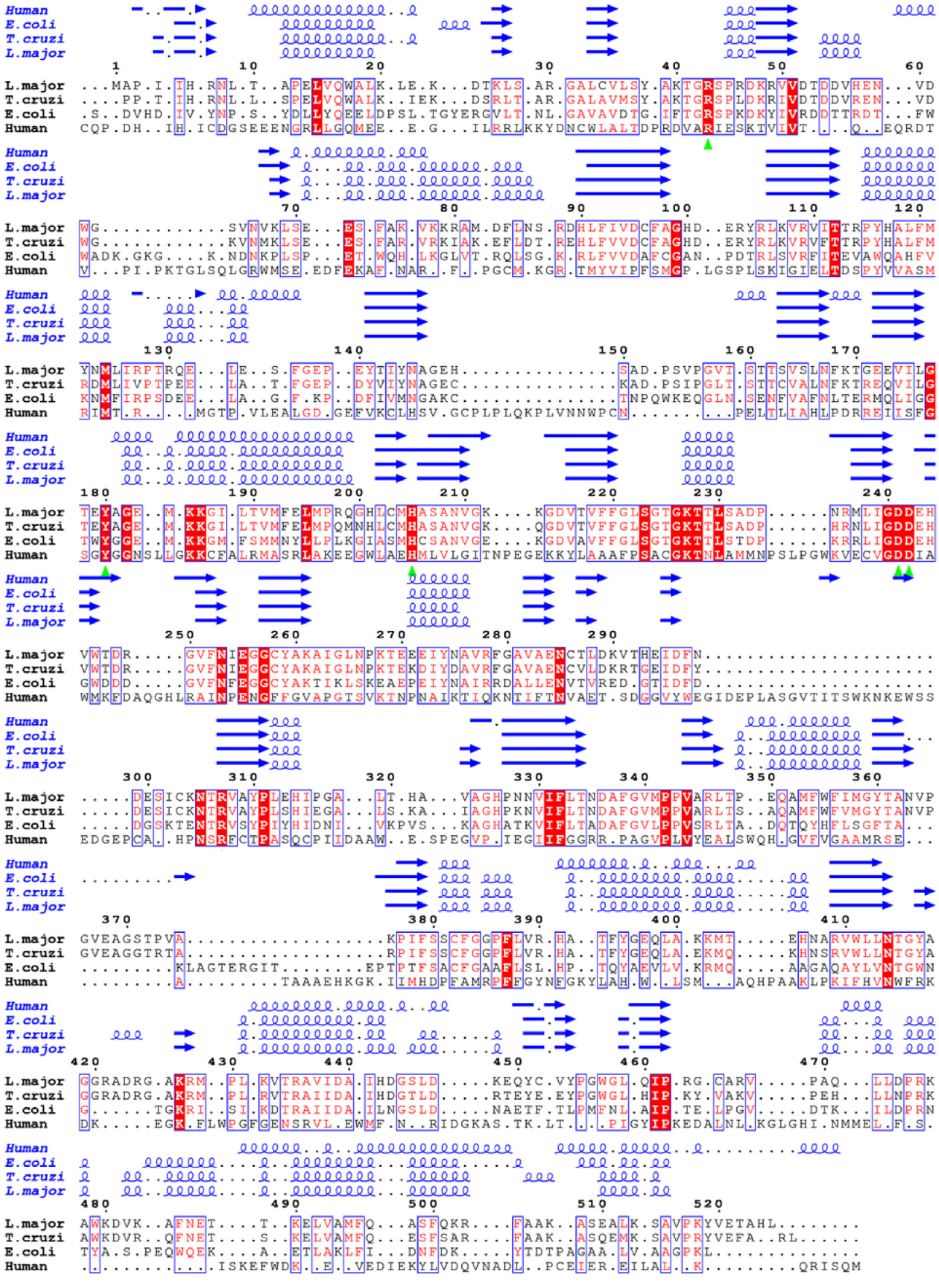
Human
E.coli
T.cruzi
L.major
L.major ...MAP.I.IH.RNL.T..APELVQWALK.LE.K...DTKLS.AR.GALCVLSY.AKTGRSPRDKRVVDTDDVHEN...VD
T.cruzi ....PP.T.IH.RNL.L..SPELVQWALK..IEK...DSRLT.AR.GALAVMSY.AKTGRSPLDKRIVDTDDVREN...VD
E.coli .S..DVHD.IV.YNP.S..YDLLYQEELDPSL.TGYERGVLT.NL.GAVAVDTG.IFTGRSPKDKYIVRDDTTRDT...FW
Human CQP.DH..IH.ICDGSEEENGRLLGQMEE..E.G...ILRRLKKYDNCWLALTDPRDVARIESKTVIVT.....Q..EQRDT
L.major WG.....SVNVKLSE...ES.FAK.VKKRAM.DFLNS.RDHLFIVDCFAGHD..ERYRLKVRVITTRPYHALFM
T.cruzi WG.....KVNMKLSE...ES.FAR.VRKIAK.EFLDT.REHLFVVDCFAGHD..ERYRLKVRVFTTRPYHALFM
E.coli WADK.GKG....K.NDNKPLSP...ET.WQH.LKGLVT.RQLSG.K.RLFVVDAFCGAN..PDTRLSVRFITEVAWQAHFV
Human V...PI.PKTGLSQLGRWMSE.EDFEKAF.NAR..F..PGCM.KGR.TMYVIPFSMGP.LGSPLSKIGIELTDSPYVVASM
L.major YNMLIRPTRQE...LE..S.FGEP..EYTIYNAGEH.....SAD.PSVPGVT.STTSVSLNFKTGEEVILG
T.cruzi RDMLIVPTPEE...LA..T.FGEP..DYVIYNAGEC.....KAD.PSIPGLT.STTCVALNFKTREQVILG
E.coli KNMFIRPSDEE...LA..G.F.KP..DFIVMNGAKC.....TNPQWKEQGLN.SENFVAFNLTERMQLIGG
Human RIMT.R...MGTP.VLEALGD.GEFVKCLHSV.GCPLPLQKPLVNNWPCN.....PELTLIAHLPDRREIISFG
L.major TEYAGE..M.KKGI.LTVMFELMPRQGHLCMHASANVGK....KGDVTVFFGLSGTGKTTLSADP.....NRMLIGDDEH
T.cruzi TEYAGE..M.KKGI.LTVMFELMPQMNHLCMHASANVGK....QGDVTVFFGLSGTGKTTLSADP.....HRNLIGDDEH
E.coli TWYGGE..M.KKGM.FSMMNYLLPLKGIASMHCSANVGE....KGDVAVFFGLSGTGKTTLSTDP.....KRRLIGDDEH
Human SGYGGNSLLGKKCFALRMASRLAKEEGWLAEHMLVLGITNPEGEKKYLAAAFPSACGKTNLAMMNPSLPGWKVECVGDDIA
L.major VWTDR.....GVFNIEGGCYAKAIGLNPKTEEEIYNAVRFGAVAENCTLDKVTHEIDFN.....
T.cruzi VWTDR.....GVFNIEGGCYAKAIGLNPKTEKDIYDAVRFGAVAENCVLDKRTGEIDFY.....
E.coli GWDDD.....GVFNFEGGCYAKTIKLSKEAEPEIYNAIRRDALLENVTVRED.GTIDFD.....
Human WMKFDAQGHLRAINPENGFFGVAPGTSVKTNPNAIKTIQKNTIFTNVAET.SDGGVYWEGIDEPLASGVTITSWKNKEWSS
L.major .....DESICKNTRVAYPLEHIPGA...LT.HA...VAGHPNNVIFLTNDAFGVMPPVARLTP..EQAMFWFIMGYTANVP
T.cruzi .....DESICKNTRVAYPLSHIEGA...LS.KA...IAGHPKNVIFLTNDAFGVMPPVARLTS..AQAMFWFVMGYTANVP
E.coli .....DGSKTENTRVSYPIYHIDNI...VKPVS...KAGHATKVIFLTADAFGVLPPVSRLTA..DQTQYHFLSGFTA...
Human EDGEPCA..HPNSRFCTPASQCPIIDAAW..E.SPEGVP.IEGIIFGGRR.PAGVPLVYEALSWQH.GVFVGAAMRSE...
L.major GVEAGSTPVA.....KPIFSSCFGGPFLVR.HA..TFYGEQLA.KKMT.....EHNARVWLLNTGYA
T.cruzi GVEAGGTRTA.....RPIFSSCFGGPFLVR.HA..TFYGEQLA.EKMQ.....KHNSRVWLLNTGYA
E.coli .....KLAGTERGIT.....EPTPTFSACFGAAFLSL.HP..TQYAEVLV.KRMQ.....AAGAQAYLVNTGWN
Human .....A.....TAAAEHKGK.IIMHDPFAMRPFFGYNFGKYLAH.W..LSM...AQHPAAKLPKIFHVNWFRK
L.major GGRADRG.AKRM..PL.KVTRAVIDA.IHDGSLD.....KEQYC.VYPGWGL.QIP.RG.CARV.....PAQ...LLDPRK
T.cruzi GGRADRG.AKRM..PL.RVTRAIIDA.IHDGTLD.....RTEYE.EYPGWGL.HIP.KY.VAKV.....PEH...LLNPRK
E.coli G.....TGKRI..SI.KDTRAIIDA.ILNGSLD.....NAETF.TLPMFNL.AIP.TE.LPGV.....DTK...ILDPRN
Human DK.....EGK.FLWPGFGENSRVL.EWMF.N..RIDGKAS.TK.LT..P.IGYIPKEDALNL.KGLGHI.NMMEL.F.S.
L.major AWKDVK..AFNET....T..KELVAMFQ...ASFQKR....FAAK..ASEALK.SAVPKYVETAHL.....
T.cruzi AWKDVR..QFNET....S..KELVAMFQ...ESFSAR....FAAK..ASQEMK.SAVPRYVEFA..RL.....
E.coli TYA.S.PEQWQEK....A..ETLAKLFI...DNFDK.....YTDTPAGAA.LV.AAGPKL.....
Human .....ISKEFWDK..E..VEDIEKYLVDQVNADL..PCEIER.EILAL..K.....QRISQM

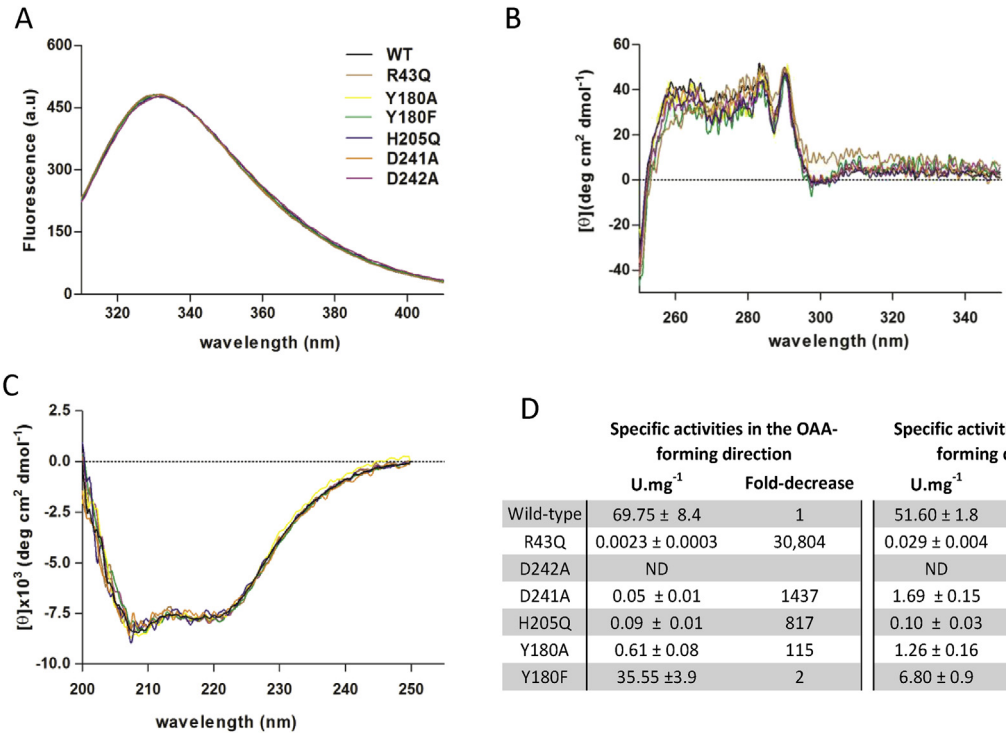

D

	Specific activities in the OAA-forming direction		Specific activities in the PEP-forming direction	
	U.mg^{-1}	Fold-decrease	U.mg^{-1}	Fold-decrease
Wild-type	69.75 ± 8.4	1	51.60 ± 1.8	1
R43Q	0.0023 ± 0.0003	30,804	0.029 ± 0.004	1,793
D242A	ND		ND	
D241A	0.05 ± 0.01	1437	1.69 ± 0.15	31
H205Q	0.09 ± 0.01	817	0.10 ± 0.03	516
Y180A	0.61 ± 0.08	115	1.26 ± 0.16	41
Y180F	35.55 ±3.9	2	6.80 ± 0.9	8

Fig. 4. Spectroscopic and functional characterization of *L. major* phosphoenolpyruvate carboxykinase mutants. **(A)** Intrinsic fluorescence, the excitation wavelength is 295 nm; **(B)** Near-UV CD spectra; **(C)** Far-UV CD spectra. All the assayed proteins were in 50 mM buffer HCl-Tris, pH 7.9, supplemented with 50 mM NaCl at concentrations indicated in Material and Methods. The color code for each protein spectrum is shown in the inset of panel A and maintained unvaried in panels B and C. **(D)** Specific activities in the OAA- and PEP-forming directions of the wild type *L. major* PEPCK and those of the analyzed mutants. ND: not detectable. Each assay was performed in triplicate using the standard assays mixtures and following the conditions described in Material and Methods.

4. Discussion

Results reported herein particularly disclose the biochemical properties of the *L. major* PEPCK as well as providing a first glimpse into this enzyme active site. Despite the fact that *L. major* PEPCK and trypanosomial counterparts reveal high sequence relatedness, interestingly our findings show that the kinetic properties of *L. major* enzyme more closely resemble those of *T. brucei* than *T. cruzi* PEPCK (For comparison see Table 2). Opposed to the *T. cruzi* enzyme, *L. major* PEPCK remains equally active in the presence or absence of reducing agents [30]. Besides, the over-all kinetic properties of *L. major* PEPCK show that like other homologues, this enzyme also exhibits the trend of catalyzing the PEP-forming reaction (gluconeogenic activity) more efficiently than PEP-carboxylation, to produce OAA (anaplerotic activity). Owing to the notable nutrient variability that trypanosomatids encounter in the different niches they colonize, PEPCK seems to be needed to guarantee the operability of Krebs cycle as well as the *de novo* synthesis of glucose in *Leishmania* spp. Therefore, this enzyme is believed to contribute to the fine tuning balance between gluconeogenesis and anaplerotic processes in the insect and mammalian stages of this pathogen [13,31,32].

3MPA has been shown to act on the *T. cruzi* PEPCK as a purely noncompetitive inhibitor in respect of the substrates corresponding to the carboxylation reaction [33]. By contrast, in the case of the *L. major* enzyme, a mixed mechanism and a classical non-competitive inhibition were observed when PEP and HCO_3^- were tested as substrates, respectively. In the case of PEP, the higher value obtained for K_{ii} than for K_{is} indicates that within the mixed inhibitory modality, the competitive component might be more prevalent than the un-competitive mechanism. This observation raises the question whether in the case of Lmj_PEPCK, 3MPA might operate as a discrete allosteric inhibitor, preventing the enzyme from achieving the catalytically competent conformation or precluding the entrance of PEP in the active site. In ATP-dependant PEPCKs, the binding site of 3MPA still remains to be disclosed. However in GTP-dependant homologues, it has been assumed that this inhibitor and PEP binds to partially overlapped sites [34].

Site directed mutagenesis studies show that the change of D242 for A renders a completely inactive enzyme, while the substitution of D241 and H205 for A and Q, respectively produces important but no so dramatic effects on Lmj_PEPCK activity. Particularly, the H205Q variant exhibits an over 250-fold increase in the apparent K_m value towards Mn^{2+} in addition to the notably lower k_{cat} values for the OAA-forming reaction (Table 1, panel B). Therefore, it is likely that as observed in the crystallographic structures of ATP- and GTP-dependant PEPCKs as well as inferred for the *T. cruzi* homologue [10,35], the side chains of the strictly conserved D241, D242 and H205 could also fulfill equivalent roles in Lmj_PEPCK.

Fig. 3. Structure-based protein sequence alignment of *L. major* phosphoenolpyruvate carboxykinase with ATP- and GTP-dependant homologues. The crystal structures of PEPCKs from *E. coli* (2PXZ.pdb), and *T. cruzi* (1Il2.pdb) were downloaded from the PDB database. Lmj_PEPCK model was generated by using MODELLER 9.12 software. The 3-dimensional structures of PEPCKs from *E. coli* (*E. coli*, 2PXZ.pdb), *T. cruzi* (T. cruzi, 1Il2.pdb) and man (Human, 1 KHB pdb) as well as the build model for Lmj_PEPCK were used to generate the structure alignment with UCSF Chimera 1.5.3 version. The first 37 and 17 amino acids from human and *E. coli* PEPCKs, respectively, were not included in the alignment. Invariant residues are highlighted by shaded red boxes while conserved residues are indicated by open blue boxes. The selected residues for site directed mutagenesis are indicated by green triangles. The figure was made with ESPrit 3.0 web tool [http://espript.ibcp.fr/ESPript/ESPript/].

Table 2
Comparison of the apparent kinetic parameters of *L. major*, *T. brucei* and *T. cruzi* PEPCKs.

	Apparent kinetic parameters in the OAA-forming direction				Apparent kinetic parameters in the PEP-forming direction			
	K_m (mM)	K_m (mM)	K_m (mM)	V_{max} (U mg^{-1})	K_m (mM)	K_m (mM)	V_{max} (U mg^{-1})	
	PEP	ADP	HCO_3^-		OAA	ATP		
L. major	0.90 ± 0.13	0.09 ± 0.01	12.3 ± 1.7	72 ± 3.5	0.09 ± 0.01	0.054 ± 0.006	49.5 ± 1.7	This work
*T. brucei	0.465 ± 0.112	0.045 ± 0.005	19 ± 2	205 ± 9	ND	ND	ND	[9]
T. brucei	0.490 ± 0.100	0.040 ± 0.011	25.7 ± 7.4	ND	0.037 ± 0.018	0.0103 ± 0.0002	ND	[8]
T. cruzi	0.035 ± 0.003	0.017 ± 0.02	2.77 ± 0.37	3.40 ± 0.18	0.044 ± 0.025	0.027 ± 0.002	32 ± 0.34	[7]
T. cruzi	0.36 ± 0.08	0.039 ± 0.001	3.7 ± 0.2	6.3	0.027 ± 0.003	0.039 ± 0.001	24	[29]

The values of the kinetic constants for PEPCK from trypanosomes were adapted from published data, references are included within the Table. *T. brucei* denotes that the kinetic parameters were determined for the recombinant enzyme and ND stands for not determined.

Interestingly, our findings show that in *L. major* PEPCK the replacement of R43 for Q and Y180 for F do not equally affect the catalytic performance of the leishmanial enzyme as identical substitutions do in ATP- (*E. coli* and yeast homologues) and GTP-dependant PEPCKs (human enzyme) [35–39]. *L. major* R43Q variant exhibits a meaningful 31000- and 1800-fold decrease in its capability of catalyzing the OAA- and PEP-forming reactions, respectively. Besides, the activity of this variant remains unresponsive when the concentrations of PEP, OAA or HCO_3^- are increased beyond those utilized in the standard reaction mixture. As compared with the wild type enzyme, this variant does not exhibit significant differences in the secondary and tertiary structures; therefore it seems likely that R43 is critical for Lmj_PEPCK activity. Given that the influence of the substitution of R for Q on the kinetic parameters could not be estimated, how R43 affects Lmj_PEPCK activity remains to be disclosed. Notably, equivalent substitution in *S. cerevisiae* PEPCK (R70Q) results in a significant but not so remarkable decrease in the rate of OAA-forming reaction (about of 4000-fold). In yeast PEPCK, the positive charge of R70 has been correlated with the catalytic mechanism as well as with PEP binding [39]. By contrast in *E. coli* PEPCK, the replacement of R65 by Q mildly raises the K_m value for PEP (11 vs 42 mM) and the k_{cat} value is about ≅ 30% lower than that of the wild enzyme. Besides in *E. coli*, kinetic and structural studies have shown that R65 jointly with Y207 (R43 and Y180 in *L. major* PEPCK) hold the CO_2 molecule in the precise location to facilitate its attack by the unstable carbanion intermediate formed when PEP is converted into OAA [36]. However, our findings show that in Lmj_PEPCK, the lack of the hydroxyl group of Y180 does not meaningfully affect the apparent K_m value for HCO_3^-.

On the other hand in rat and human GTP-dependant PEPCKs, the guanidine group of R87 and the positively charged edge of the aromatic ring of Y235 (equivalent to R43 and Y180 in Lmj_PEPCK) are mainly involved in counterbalancing the negative charges of PEP phosphate and carboxylate groups [40,41]. In human PEPCK, the substitution of Y235 for F remarkably influences the OAA forming activity. The V_{max} of this mutant is about 10% of the value determined for the wild type enzyme, being the apparent K_m value for Mn^{2+} notably increased, while that for PEP significantly lowered [37]. By contrast, our findings show that in *L. major* PEPCK, the substitution of Y180 for F affects PEP- more significantly than OAA-forming activity, remaining unaltered the apparent K_m values for the substrates and Mn^{2+}. Alternatively, when Y180 is replaced for A, the K_m value towards Mn^{2+} increases in about 10-fold. Besides opposed to the human variant, when in Lmj_PEPCK Y180 is substituted for F or A the apparent K_m values towards HCO_3^- and PEP remain nearly unaltered (Table 1, panels C and D). These findings suggest that unlike in human enzyme [37], the aromatic ring of Y180 might not establish an anion–quadrupole interaction with PEP in Lmj_PEPCK.

In summary, it appears that R43 and Y180 play relevant roles even in the catalytic mechanism or in the transition rates from the open state to the closed and catalytically competent form of *L. major* PEPCK. Unexpectedly, the lack of the aromatic ring in the position of Y180 only significantly increases the apparent K_m value for Mn^{2+} and diminishes the rates of both PEP- and OAA-production. These findings indicate that further structural and biochemical studies are needed to better understand the roles played by R43 and Y180. These residues could be directly involved in the catalytic mechanism or/and comprised among those involved in the substrate induced fit required to reach the final key-lock or active enzyme conformation. In order to shed light on the particularities of leishmanial PEPCKs, new approaches are currently under way in our laboratory.

Acknowledgments

This work was performed with grants to CN from Universidad de Buenos Aires (UBACYT 20100100618) and Agencia Nacional de Promoción Científica y Tecnológica (ANPCYT, Argentina, PICT 2008-0219). We are indebted to Dr. Gabriela Gómez for her invaluable help with the circular dichroism spectroscopy analysis. CN is a member of the Research Career from CONICET; MHS and LG are PhD students supported by UBA and CONICET respectively.

Appendix A. Supplementary data

Supplementary data related to this article can be found at http://dx.doi.org/10.1016/j.abb.2015.07.015.

References

[1] W.H.Organization, http://www.who.int/mediacentre/factsheets/fs375/en/index.html, 2013.
[2] S.L. Croft, P. Olliaro, Leishmaniasis chemotherapy-challenges and opportunities, Clin. Microbiol. Infect. 17 (2011) 1478–1483.
[3] J. Yang, S.C. Kalhan, R.W. Hanson, What is the metabolic role of phosphoenolpyruvate carboxykinase? J. Biol. Chem. 284 (2009) 27025–27029.
[4] A. Matte, L.W. Tari, H. Goldie, L.T. Delbaere, Structure and mechanism of phosphoenolpyruvate carboxykinase, J. Biol. Chem. 272 (1997) 8105–8108.
[5] L.T. Delbaere, A.M. Sudom, L. Prasad, Y. Leduc, H. Goldie, Structure/function studies of phosphoryl transfer by phosphoenolpyruvate carboxykinase, Biochim. Biophys. Acta 1697 (2004) 271–278.
[6] G.M. Carlson, T. Holyoak, Structural insights into the mechanism of phosphoenolpyruvate carboxykinase catalysis, J. Biol. Chem. 284 (2009) 27037–27041.
[7] C. Cymeryng, J.J. Cazzulo, J.J. Cannata, Phosphoenolpyruvate carboxykinase from *Trypanosoma cruzi*. Purification and physicochemical and kinetic properties, Mol. Biochem. Parasitol. 73 (1995) 91–101.
[8] M. Hunt, P. Köhler, Purification and characterization of phosphoenolpyruvate carboxykinase from *Trypanosoma brucei*, Biochim. Biophys. Acta 1249 (1995) 15–22.
[9] A. Yévenes, E. Cardemil, Expression of the *Trypanosoma brucei* phosphoenolpyruvate carboxykinase gene in *Saccharomyces cerevisiae*, Biochimie 2 (2000) 123–127.

[10] S. Trapani, J. Linss, S. Goldenberg, H. Fischer, A.F. Craievich, G. Oliva, Crystal structure of the dimeric phosphoenolpyruvate carboxykinase (PEPCK) from *Trypanosoma cruzi* at 2 A resolution, J. Mol. Biol. 313 (2001) 1059–1072.
[11] B. Szöör, J.R. Haanstra, M. Gualdrón-López, P.A. Michels, Evolution, dynamics and specialized functions of glycosomes in metabolism and development of trypanosomatids, Curr. Opin. Microbiol. 22C (2014) 79–87.
[12] E.C. Saunders, W.W. Ng, J.M. Chambers, M. Ng, T. Naderer, J.O. Krömer, V.A. Likic, M.J. McConville, Isotopomer profiling of *Leishmania mexicana* promastigotes reveals important roles for succinate fermentation and aspartate uptake in tricarboxylic acid cycle (TCA) anaplerosis, glutamate synthesis, and growth, J. Biol. Chem. 286 (2011) 27706–27717.
[13] E.C. Saunders, W.W. Ng, J. Kloehn, J.M. Chambers, M. Ng, M.J. McConville, Induction of a stringent metabolic response in intracellular stages of *Leishmania mexicana* leads to increased dependence on mitochondrial metabolism, PLoS Pathog. (2014) e1003888 doi:10.1371.
[14] D. Rodriguez-Contreras, N. Hamilton, Gluconeogenesis in *Leishmania mexicana*: contribution of glycerol kinase, phosphoenolpyruvate carboxykinase, and pyruvate phosphate dikinase, J. Biol. Chem. 289 (2014) 32989–33000.
[15] D.J. Creek, M. Mazet, F. Achcar, J. Anderson, D.H. Kim, R. Kamour, P. Morand, Y. Millerioux, M. Biran, E.J. Kerkhoven, A. Chokkathukalam, S.K. Weidt, K.E. Burgess, R. Breitling, D.G.1 Watson, F. Bringaud, M.P. Barrett, Probing the metabolic network in bloodstream-form *Trypanosoma brucei* using untargeted metabolomics with stable isotope labelled glucose, PLoS Pathog. 16 11 (3) (2015) e1004689.
[16] J.C. Mottram, G.H. Coombs, *Leishmania mexicana*: Enzyme activities of amastigotes and promastigotes and their inhibition by antimonials and arsenicals, Exp. Parasitol. 59 (1985) 151–160.
[17] P.G. Nugent, S.A. Karsani, R. Wait, J. Tempero, D.F. Smith, Proteomic analysis of *Leishmania mexicana* differentiation, Mol. Biochem. Parasitol. 136 (2004) 51–62.
[18] D. Paape, M.E. Barrios-Llerena, T. Le Bihan, L. Mackay, T. Aebischer, Gel free analysis of the proteome of intracellular *Leishmania mexicana*, Mol. Biochem. Parasitol. 169 (2010) 108–114.
[19] M.C. Brotherton, G. Racine, A.L. Foucher, J. Drummelsmith, B. Papadopoulou, M. Ouellette, Analysis of stage-specific expression of basic proteins in *Leishmania infantum*, J. Proteome Res. 9 (2010) 3842–3853.
[20] E. Medina-Acosta, G.A. Cross, Rapid isolation of DNA from trypanosomatid protozoa using a simple 'mini-prep' procedure, Mol. Biochem. Parasitol. 59 (1993) 327–329.
[21] H. Schägger, G. von Jagow, Tricine-sodium dodecyl sulfate-polyacrylamide gel electrophoresis for the separation of proteins in the range from 1 to 100 kDa, Anal. Biochem. 166 (1987) 368–379.
[22] M.M. Bradford, A rapid and sensitive method for the quantitation of microgram quantities of protein utilizing the principle of protein-dye binding, Anal. Biochem. 72 (1976) 248–254.
[23] R.A. Copeland, Enzymes: a Practical Introduction to Structure, Mechanism, and Data Analysis, Wiley-VCH, Inc, 2000 (Chapter 8).
[24] H.J. Motulsky, A. Christopoulos, Fitting Models to Biological Data Using Linear and Nonlinear Regression, GraphPad Software Inc., San Diego, CA, 2003.
[25] R.A. Laskowski, M.W. MacArthur, D.S. Moss, J.M. Thornton, PROCHECK: a program to check the stereochemical quality of protein structures, J. Appl. Cryst. 26 (1993) 283–291.
[26] D.R. Eisenberg, Luthy, et al., VERIFY3D: assessment of protein models with three-dimensional profiles, Methods Enzymol. 277 (1997) 396–404.
[27] E.F. Pettersen, T.D. Goddard, C.C. Huang, G.S. Couch, D.M. Greenblatt, E.C. Meng, T.E. Ferrin, Chimera-a visualization system for exploratory research and analysis, J. Comput. Chem. 13 (2004) 1605–1612.
[28] P. Gouet, X. Robert, E. Courcelle, ESPript/ENDscript: extracting and rendering sequence and 3D information from atomic structures of proteins, Nucleic Acids Res. 31 (2003) 3320–3323.
[29] J.A. Urbina, The phosphoenolpyruvate carboxykinase of Trypanosoma (Schizotrypanum) cruzi epimastigotes: molecular, kinetic, and regulatory properties, Arch. Biochem. Biophys. 258 (1987) 186–195.
[30] L.A. Jurado, I. Machín, J.A. Urbina, *Trypanosoma cruzi* phosphoenolpyruvate carboxykinase (ATP-dependent): transition metal ion requirement for activity and sulfhydryl group reactivity, Biochim. Biophys. Acta 1292 (1996) 188–196.
[31] M.J. McConville, T. Naderer, Metabolic pathways required for the intracellular survival of *Leishmania*, Annu. Rev. Microbiol. 65 (2011) 543–561.
[32] D. Rosenzweig, D. Smith, F. Opperdoes, S. Stern, R.W. Olafson, D. Zilberstein, Retooling *Leishmania* metabolism: from sand fly gut to human macrophage, FASEB J. 22 (2008) 590–602.
[33] J.A. Urbina, C.E. Osorno, A. Rojas, Inhibition of phosphoenolpyruvate carboxykinase from *Trypanosoma (Schizotrypanum) cruzi* epimastigotes by 3-mercaptopicolinic acid: *in vitro* and *in vivo* studies, Arch. Biochem. Biophys. 282 (1990) 91–99.
[34] A.L. Makinen, T. Nowak, 3-Mercaptopicolinate. A reversible active site inhibitor of avian liver phosphoenolpyruvate carboxykinase, J. Biol. Chem. 258 (1983) 11654–11662.
[35] L.W. Tari, A. Matte, H. Goldie, L.T. Delbaere, Mg(2+)-Mn2+ clusters in enzyme-catalyzed phosphoryl-transfer reactions, Nat. Struct. Biol. 12 (1997) 990–994.
[36] J.J. Cotelesage, J. Puttick, H. Goldie, B. Rajabi, B. Novakovski, L.T. Delbaere, How does an enzyme recognize CO_2? Int. J. Biochem. Cell. Biol. 39 (2007) 1204–1210.
[37] L. Dharmarajan, C.L. Case, P. Dunten, B. Mukhopadhyay, Tyr235 of human cytosolic phosphoenolpyruvate carboxykinase influences catalysis through an anion-quadrupole interaction with phosphoenolpyruvate carboxylate, FEBS J. 275 (2008) 5810–5819.
[38] C. Andrade, C. Sepulveda, E. Cardemil, A.M. Jabalquinto, The role of tyrosine 207 in the reaction catalyzed by *Saccharomyces cerevisiae* phosphoenolpyruvate carboxykinase, Biol. Res. 43 (2010) 191–195.
[39] C.M. Ravanal, M. Flores, E. Pérez, F. Aroca, E. Cardemil, *Saccharomyces cerevisiae* phosphoenolpyruvate carboxykinase: relevance of arginine 70 for catalysis, Biochimie 86 (2004) 357–362.
[40] P. Dunten, C. Belunis, R. Crowther, K. Hollfelder, U. Kammlott, W. Levin, H. Michel, G.B. Ramsey, A. Swain, D. Weber, S.J. Wertheimer, Crystal structure of human cytosolic phosphoenolpyruvate carboxykinase reveals a new GTP-binding site, J. Mol. Biol. 316 (2002) 257–264.
[41] S. Sullivan, T. Holyoak, Structures of rat cytosolic PEPCK: insight into the mechanism of phosphorylation and decarboxylation of oxaloacetic acid, Biochemistry 46 (2007) 10078–10088.